(Received 20 October 2023, Accepted 27 May 2024, Scheduled 5 June 2024)

Fabricated Magnetic-Dielectric Synergy Fe@Carbon Microspheres by Spray-Pyrolysis with Excellent Microwave Absorption in C-Band

Hao Zhu[1], Zhuolin Li[1], Mengqiu Huang[2], Lei Wang[4,*], Yuxiang Lai[5], Yongsheng Liu[1,3,*], and Renchao Che[2,3,*]

[1] *Institute of Solar Energy, Shanghai University of Electric Power, Shanghai 200090, China*
[2] *Laboratory of Advanced Materials, Shanghai Key Lab of Molecular Catalysis and Innovative Materials Academy for Engineering & Technology, Fudan University, Shanghai 200438, P. R. China*
[3] *Zhejiang Laboratory, Hangzhou 311100, P. R. China*
[4] *School of Materials Science and Engineering, Shanghai Institute of Technology, Shanghai 201418, China*
[5] *Pico Electron Microscopy Center; Innovation Institute for Ocean Materials Characterization Center for Advanced Studies in Precision Instruments, Hainan University, Haikou 570228, China*

ABSTRACT: The development of materials with excellent absorption properties in the C-band through the utilization of the magnetoelectric coupling effect holds great potential within the field of absorption research. However, there are still several challenges. To address these challenges, Fe@Carbon (Fe@C) microspheres were successfully fabricated using spray-drying followed by pyrolysis. The average size of the Fe@C microspheres is 3.6 μm with uniform dispersion, where iron nanoparticles (NPs) are tightly anchored with the carbon matrix to tune the microwave absorption properties. Synthesized Fe@C microspheres exhibit remarkable electromagnetic wave absorption capability within the C-band (4–8 GHz), covering a bandwidth of 2.8 GHz. Also, the Fe@C microsphere exhibits a minimum reflection loss of −48.11 dB at 4.5 mm thickness and 6.88 GHz. Systematic analysis has uncovered that the integration of large-sized magnetic carbon structures, high-density confinement of magnetic units, and robust magnetic coupling are crucial for enhancing the magnetic loss dissipation. This study introduces a novel approach for the preparation of electromagnetic absorbing materials, providing inspiration for further exploration of the mechanism behind low-frequency magnetic loss.

1. INTRODUCTION

The advancement of 5G technology has accelerated the utilization of high-frequency electric devices and artificial intelligence, but it has also resulted in a growing concern regarding the escalation of electromagnetic pollution. The 5G EM wave primarily occupies the C-band (4–8 GHz) and is classified as a high-frequency electromagnetic wave (2–18 GHz). Therefore, the production of electromagnetic wave absorption materials is necessary to mitigate the pollution caused by 5G equipment's electromagnetic radiation. Electromagnetic wave absorption materials are typically divided into magnetic loss materials and dielectric loss materials [1]. Despite extensive research on electromagnetic wave absorption materials such as magnetic metals and metal oxides, these materials have limitations concerning their absorption frequency and bandwidth capability [2]. Consequently, recent research efforts have been concentrated on identifying more effective solutions by integrating magnetic materials with lightweight conductive materials to improve absorption performance. One notable example of these explorations is the combination of magnetic nanoparticles with carbon-based materials, including graphene and carbon nanotubes [3]. This innovative approach has demonstrated great promise in enhancing the performance of electromagnetic wave absorption. In order to obtain the desired-frequency for electromagnetic absorption, numerous preparation methods have been discovered to the magnetic-carbon system, such as hydrothermal synthesis [4], pyrolysis [5], electrospinning [6], chemical condensation [7], reduction [8], melting [9], vapor deposition [10], solution pulsed laser irradiation [11], arc plasma combustion [12], and arc discharge [13]. Meanwhile, microstructure and dimensional regulation was also applied in the iron-carbon-based composites to tune the magnetic and dielectric absorption by adjusting the magnetic properties and chemistry environment. For example, rose-like Fe@C hollow microspheres [14], carbon-coated Fe particles [15], 1D Fe/C fiber chains [16], Fe/C nano cubic [17], Fe/CNTs [18], onion-like carbon-encapsulated Fe particles [19], Fe/C nanosheets [20], yolk-shell structured 2D sheet-like Fe/vacancy/C [21], and 3D porous Fe/C composite material [22].

In this study, spray pyrolysis was employed to compound Fe NPs with magnetic loss and carbon with dielectric loss, respectively. Through the modulation of fabrication conditions, it is possible to refine the size, morphology, and dispersion of the microspheres. The modification of these microspheres can be utilized to adjust the electromagnetic parameters, leading to

* Corresponding authors: Lei Wang (leiwang@sit.edu.cn); Yongsheng Liu (ysliu@shiep.edu.cn); Renchao Che (rcche@fudan.edu.cn).

a significant enhancement of EM energy absorption. The inherent strong resonance of Fe NPs significantly contributes to superior magnetic loss properties, while carbon microspheres with defects exhibit remarkable dielectric loss features. By manipulating the ratio between the iron source and melamine, it is possible to adjust the relative content of Fe NPs and carbon spheres, achieving optimal impedance matching. This manipulation results in a synergistic effect that enhances EM energy absorption capabilities. Fe@C-1 demonstrated a noteworthy minimum reflection loss (RL_{min}) of -48.11 dB, and the EM wave absorption bandwidth (*EAB*) spanned almost 70% of the C-band. In brief, the Fe@C microspheres synthesized via spray pyrolysis present several advantages, including facile large-scale production, exceptional dispersibility, and notable electromagnetic wave absorption capabilities within the C-band frequency range.

2. EXPERIMENTAL SECTION

2.1. Materials

Iron (III) nitrate nonahydrate (Fe $(NO_3)_3 \cdot 9H_2O$, AR), N, N-dimethylformamide (DMF), anhydrous ethanol, and Polyvinylpyrrolidone (PVP) were procured from Shanghai Sinopharm Chemical Reagent Co., Ltd., and were of analytical reagent grade. The chemicals were utilized in their original form. Milli-Q water, generated by the Milli-Q system (Millipore, Bedford, MA), was employed in all experimental procedures.

2.2. Synthesis of the Precursor Powders

The synthesis process began with the addition of 0.808 g of Fe $(NO_3)_3 \cdot 9H_2O$ and 1.5 g of PVP K30 into a mixed solution composed of deionized water (10 mL), ethanol (10 mL), and N, N-dimethylformamide (10 mL). Following magnetic stirring for 30 minutes, the precursors were prepared for the next stage by undergoing the spray drying process. The spray drying was conducted with carefully optimized parameters: an inlet temperature of 180°, an outlet temperature of 97°, and a solution flow rate into the spray nozzle set at 20 revolutions per second. Upon completion of the spray drying process yellow precursor powders were produced.

2.3. Synthesis of the Fe@C Microspheres

The yellow powders (0.8 g) were mixed with different quantities of melamine (0.4 g, 0.8 g, and 1.2 g) correspondingly. The resulting mixtures were subsequently pyrolyzed at 600° for 300 minutes under a H_2/Ar atmosphere, with a heating rate of 2°C/min. The final composites were designated as Fe@C-1, Fe@C-2, and Fe@C-3, respectively.

2.4. Characterization

The phase analysis of Fe@C microspheres was conducted using a Bruker D8-Advance X-ray diffractometer (Germany). To assess the size and morphology of the Fe@C samples, a field-emission scanning electron microscope (FESEM, S-4800) and a field-emission transmission electron microscope (TEM, JEOL, JEM-2100F) were used. Raman spectra were acquired by the Renishaw Invia spectrometer. X-ray Photoelectron Spectroscopy (XPS) measurements were performed on a Thermo Scientific ESCALAB 250Xi spectrometer device. The EM parameters were evaluated using an N5230C vector network analyzer at 2–18 GHz. To prepare the measured samples, the absorbents were uniformly mixed with a paraffin matrix at a mass fraction of 60%, and subsequently compacted into columnar rings with an outer diameter of 7.00 mm and an inner diameter of 3.04 mm. The calculation of *RL* and impedance matching was performed using the specified formula [23]:

$$Z = |Z_{in}/Z_o| = \sqrt{|\frac{\mu_r}{\varepsilon_r}|} \tan h \left[j \left(\frac{2\pi f d}{c} \right) \sqrt{\mu_r \varepsilon_r} \right]$$

$$RL = 20 \left| \left(\log \left(Z_{in} - Z_o \right) / \left(Z_{in} + Z_o \right) \right) \right|$$

3. RESULTS AND DISCUSSION

The preparation process for Fe@C microspheres is depicted in Figure 1(a). At the outset, a mixed solution containing a ferric source and polyvinylpyrrolidone is employed for magnetic stirring. This initial step ensures thorough dissolution and contributes to the prevention of agglomeration [24–27]. Then, the solution is subjected to a spray-drying process to produce precursor powders. During this process, the solution is atomized through a nozzle, resulting in the formation of tiny droplets that quickly evaporate their internal solvent upon exposure to hot air. Subsequently, the precursor powders were combined with melamine in various mass ratios. The resulting mixtures were then kept at a temperature of 600°C for a duration of 300 minutes. This thermal treatment was crucial in the formation of Fe@C microspheres with enhanced electromagnetic properties. Finally, the precursor powders were transformed into Fe@C microspheres. In Figure 1(b), the peak observed at $2\theta = 44.6°$ corresponds to the (110) plane of iron [27–29]. Additionally, the XRD spectrum indicates the presence of a diffraction peak at $2\theta = 25.8°$, which is indicative of an amorphous carbon composition. The intensity of the carbon peak becomes more evident with an increase in the mass of melamine, indicating the modification of carbon crystallinity. The addition of melamine influences the structural properties of the carbon component in the Fe@C microspheres. Conversely, the intensity of the iron peak progressively diminishes, implying that the incorporation of melamine stimulates the growth of the carbon matrix and impedes the formation of iron metal particles. Raman spectroscopy is commonly employed to analyze the graphitized degree of carbon materials. The D-band is associated with disordered graphite materials or defects in graphite [30], whereas the G-band corresponds to the vibration of sp^2 hybridized carbon atoms [31–33]. The I_D/I_G value is employed as an indicator to evaluate the extent of graphitization of the carbon component [34]. As illustrated in Figure 1(c), the I_D/I_G values for the Fe@C-1, Fe@C-2, and Fe@C-3 microspheres are 1.07, 1.13, and 1.15, respectively. These values indicate varying degrees of graphitization within the carbon structure. Among these microspheres, Fe@C-1 exhibits the lowest I_D/I_G ratio, signifying the highest degree of graphitization in the carbon structure.

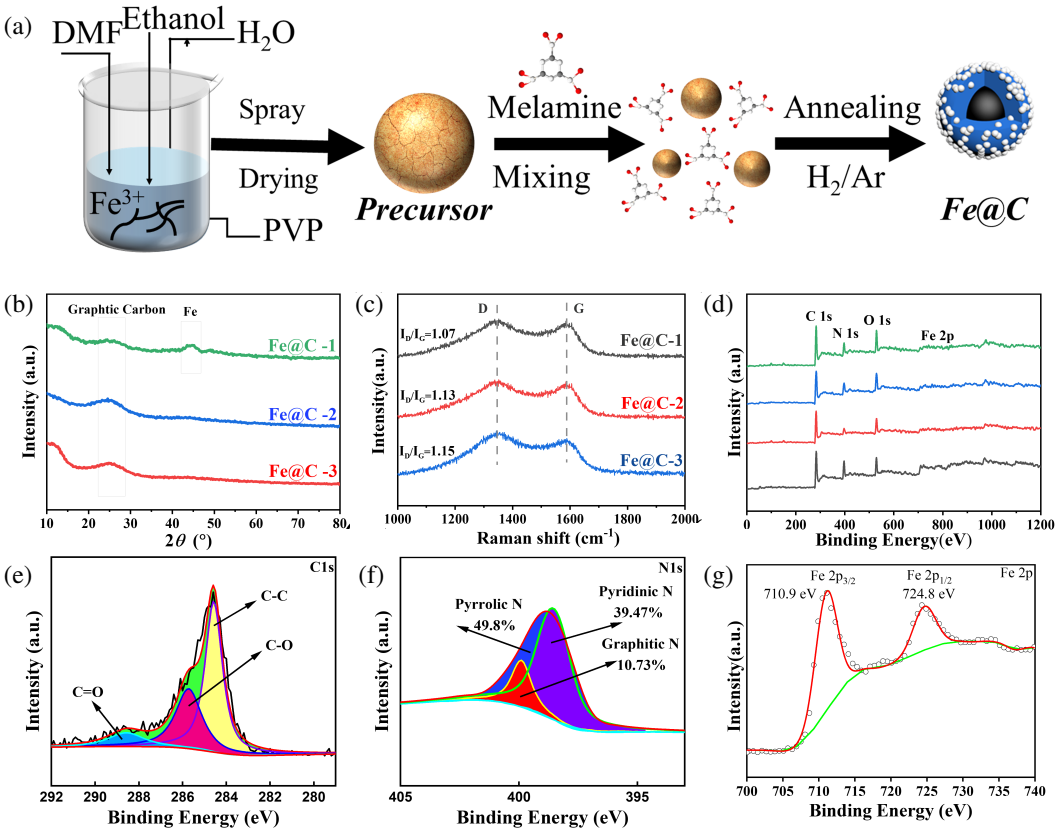


FIGURE 1. (a) Schematic illustration for Fe@C microspheres production; (b) XRD pattern and (c) Raman spectrum of Fe@C-x microspheres, (d) XPS survey spectra and XPS spectra of (e) C, (f) N, (g) Fe 2p.

This observation further supports the influence of melamine content on the structural properties of the Fe@C microspheres.

The XPS spectrum was depicted in Figure 1(d) to disclose the chemical environment in the Fe@C microspheres. In the C1s spectrum (Figure 1(e)), three distinguishable peaks are apparent at 284.6 eV, 285.4 eV, and 287.8 eV, which correspond to the C-C, C-O, and C=O bonds. As shown in Figure 1(f), the Fe@C microspheres contain three distinct types of nitrogen atoms: pyridinic-N, pyrrolic-N, and graphitic-N. The presence of these nitrogen groups is indicative of the diverse chemical environments within the microspheres, which can impact inherent electromagnetic properties. The Fe 2p spectrum depicted in Figure 1(g) exhibits two peaks at 710.9 eV and 724.8 eV, representing to the Fe $2p_{3/2}$ and Fe $2p_{1/2}$, respectively. These peaks provide valuable information regarding the state and chemical bonding in the Fe@C microspheres.

The morphology and size distribution of the Fe@C microspheres are presented in Figure 2. It is apparent from the images presented in Figures 2(a), (d), (g) that the Fe@C composites possess a remarkable feature of uniform dispersibility. Additionally, the microspheres exhibit smooth surfaces and a well-defined spherical shape, as depicted in the high-resolution images (Figures 2(b), 2(e), 2(h)). In addition, it is evident that the Fe NPs are intricately embedded within the carbon spheres, with a diminishing trend noticeable from Fe@C-1 to Fe@C-3. The size distributions of the Fe@C microspheres were calculated and presented in Figures 2(c), 2(f), and 2(i). The microspheres are characterized by dimensions within the micrometer scale, with average sizes varying between 3.4 to 3.6 µm. These results further support the well-controlled and reproducible nature of the synthesis process, leading to the formation of uniform microspheres with precise morphologies and sizes. Furthermore, the energy-dispersive X-ray spectrometry (EDS) mapping of Fe@C-1 illustrates the uniform dispersion of Fe, N, and C elements.

Figures 3(a) and 3(b) depict the TEM images of as-prepared Fe@C-1 microspheres, which exhibit a spherical shape consistent with the SEM images. The high-density Fe NPs is clearly embedded within the carbon matrix, as seen in Figures 2(c) and 2(b). From Figures 3(c) and 3(d), it is apparent that the Fe particles are relatively well-dispersed within the matrix, and the size of the Fe particles is estimated to be approximately 14.54 nm based on particle size statistics. In Figure 3(e), the spacing values of 0.20 nm and 0.17 nm correspond to the (111) and (200) planes of the Fe, respectively. This finding unambiguously confirms the presence of metallic Fe (JCPDS No. 88-2324) providing robust evidence of the Fe phase within the Fe@C microspheres.

According to the transmission line theory, the EM parameters ($\varepsilon_r = \varepsilon' - j\varepsilon''$, $\mu_r = \mu' - j\mu''$) were measured and applied to calculate the *RL* curves. The real part (ε', μ') of the EM parameters represents the storage capability of the material for

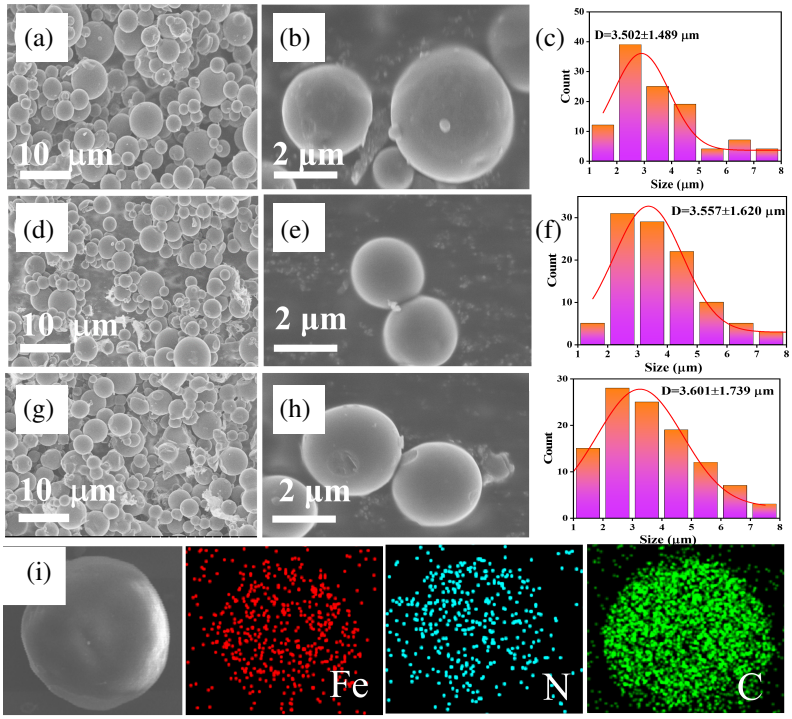


FIGURE 2. SEM images for (a), (b) Fe@C-1, (d), (e) Fe@C-2, (g)–(h) Fe@C-3; (c), (f), (i) the size distribution of Fe@C-1 to Fe@C-3; (j) the EDS of Fe@C-1.

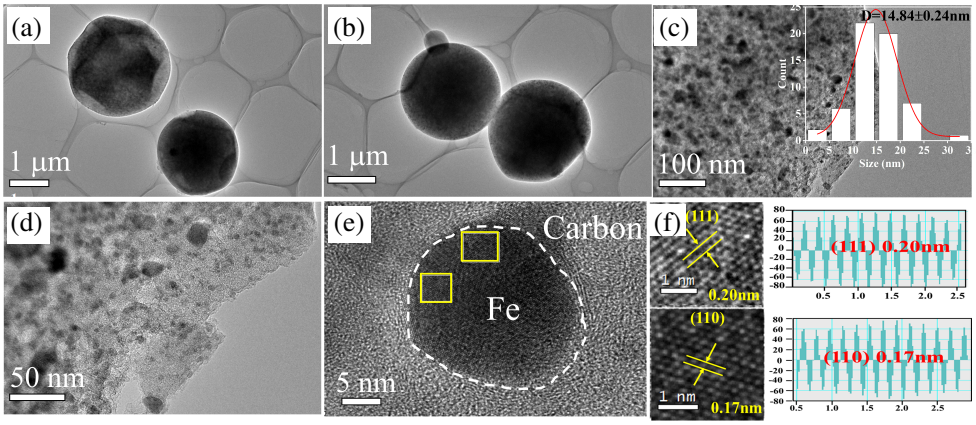


FIGURE 3. (a), (b) TEM and HRTEM images of Fe@C-1; the size distribution Fe NPs is inserted in the Figure 3(c), the lattice spacing files are inserted in Figure 3(f).

incident EM wave energy, while the imaginary part (ε'', μ'') indicates the material's dielectric ability and absorption capability. The loss angle tangent values ($\tan\delta_\varepsilon$, $\tan\delta_\mu$) reflect the energy loss during the transmission of electromagnetic waves.

From Figure 4(a), the ε' and ε'' values of Fe@C-1 range from 8.5 to 5.6 and 4.6 to 2.3, respectively. As the melamine content increases, both the real and imaginary parts of the complex permittivity values decrease. For Fe@C-3, the ε' values decrease from 6.1 to 5.3, and the ε'' values change from 1.4 to 0.8. The dielectric loss $\tan\delta_\varepsilon$ ($\tan\delta_\varepsilon = \varepsilon''/\varepsilon'$) in Figure 4(d) is used to estimate the dielectric loss ability. The values of $\tan\delta_\varepsilon$ alter from 0.52 in Fe@C-1 to 0.23 in Fe@C-3. The decline can be attributed to the inhibitory effect of increased melamine on the growth of Fe metal particles and the promoting effect on the growth of amorphous carbon. In Figure 4(d) it can be observed that the values of μ' change from 1.3 in Fe@C-1 to 1.1 in Fe@C-3, while Fe@C-1 exhibits the highest μ'' value of 0.42. The magnetic loss tangent ($\tan\delta_\mu$) values exhibit a similar trend to μ'. Generally, Fe@C-1 demonstrates the highest value of $\tan\delta_\mu$, indicating that the Fe@C microspheres possess a strong magnetic loss ability. From the Cole-Cole plots (Figures 4(g), (h), (i)), the polarization relaxation performance in Fe@C microspheres can enhance the dielectric loss. In conclusion, the study on absorption properties reveal that the electromagnetic characteristics of Fe@C microspheres are influenced by tuning the melamine content. These findings provide crucial insights

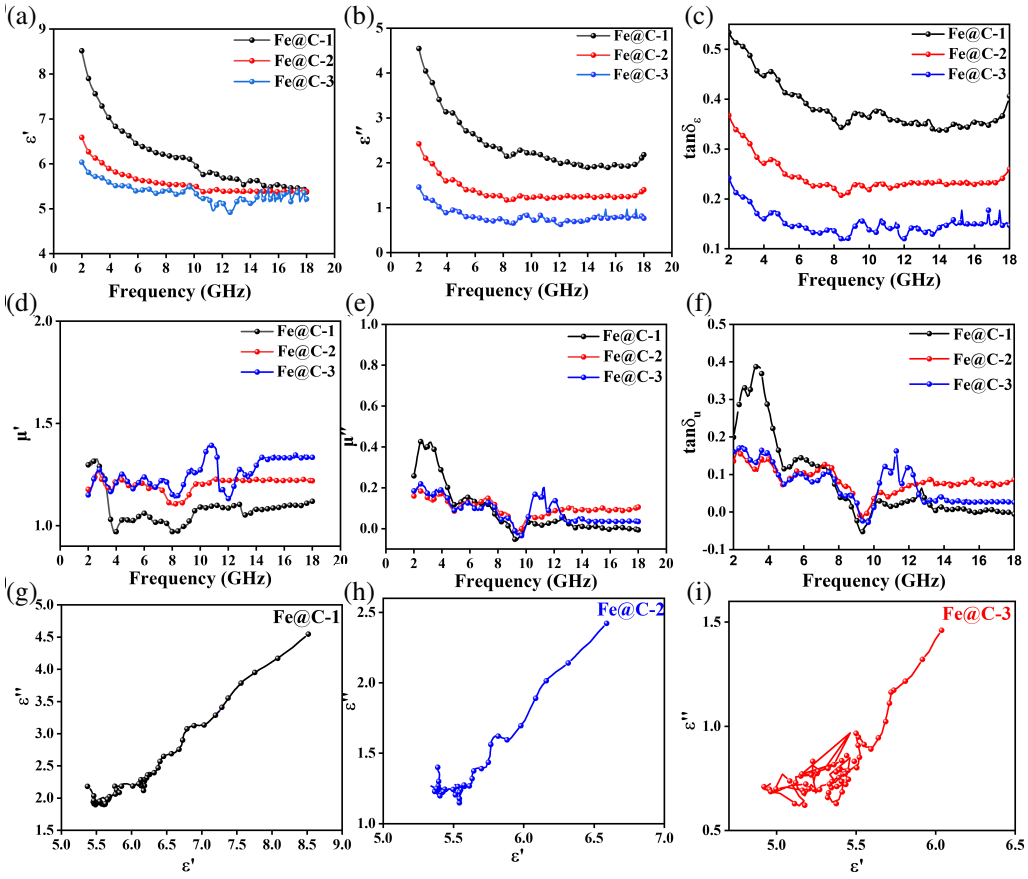


FIGURE 4. (a) Real part (ε'), (b) imaginary part (ε''), (c) tan δ_ε value, (d) real part (μ'), (e) imaginary part (μ'') (f) tan δ_μ value of Fe@C-x composites the ColeCole plots for (g) Fe@C-1, (h) Fe@C-2 and (i) Fe@C-3 microsphere.

for a comprehensive understanding of the absorption properties of Fe@C microspheres.

The *RL* values of Fe@C microspheres are calculated based on the measured permittivity and permeability, which play a crucial role on final absorption performance. The absorption performance map, illustrating the absorption characteristics, is displayed in Figure 5.

According to Figure 5, it can be observed that the *RL* curves gradually decrease as the carbon content increases (Figures 5(a), (d), (h)). Fe@C-1 microspheres exhibit the strongest *RL* among the microspheres in the C-band, reaching a $RL_{\min}$ value of -48.11 dB. When the thickness is 4.5 mm, the efficient absorption bandwidth is 2.8 GHz within the C-band. (Figures 5(b), 5(c)).

By adjusting the composition of Fe@C microspheres, the *RL* of Fe@C-2 decreased to -32.77 dB (Figures 5(e), 5(f)). Interestingly, the microspheres realized their lowest *RL* at 1.8 mm thickness. This finding implies that the melamine content may be manipulated to optimize the thickness for specific applications, potentially leading to thinner and more efficient materials. On the other hand, Fe@C-3 exhibited the minimum *RL* of -24.73 dB at a thickness of 5.0 mm. For Fe@C-1 microspheres, the real part (ε') and imaginary part (ε'') of the permittivity in the C-band (4–8 GHz) decreased from 6.4 to 6.1 and 3.2 to 2.4, respectively. Similarly, the real part (μ') and imaginary part (μ'') of the permeability changed from 1.1 to 1.2 and 0.3 to 0.1. The minimum values of *RL* and *EAB* were -48.11 dB and 2.8 GHz, respectively. In conclusion, as the melamine content increases, the thickness of the minimum *RL* undergoes a transition from reduction to enhancement. Conversely, the $RL_{\min}$ values decline as the carbon content increases. It is crucial to thoroughly investigate the optimal balance point among material composition, thickness, and electromagnetic parameters to attain the low-frequency microwave absorption in C-band.

In Figure 6, related absorption loss mechanism is demonstrated. The main reason for the microwave absorption can be attributed to the magnetic Fe NPs, and carbon components Magnetic Fe NPs induce magnetic loss due to variations in the magnetic field, leading to a reorganization of the magnetic domains [35–37]. The restructuring process results in the consumption of energy from the magnetic field, transforming it into heat energy. Natural resonance occurs when the frequency of the electromagnetic field aligns with the motion of the magnetic moment, resulting in magnetic loss [38, 39]. Dimensional resonance, exchange resonance, domain wall resonance, and exchange harmonics, which arise from the spin motion of three-dimensional electrons, also lead to some degree of loss. The second mechanism is attributed to the interaction between the three-dimensional electrons and the electromagnetic field. This interaction generates magnetic eddy currents, which in turn

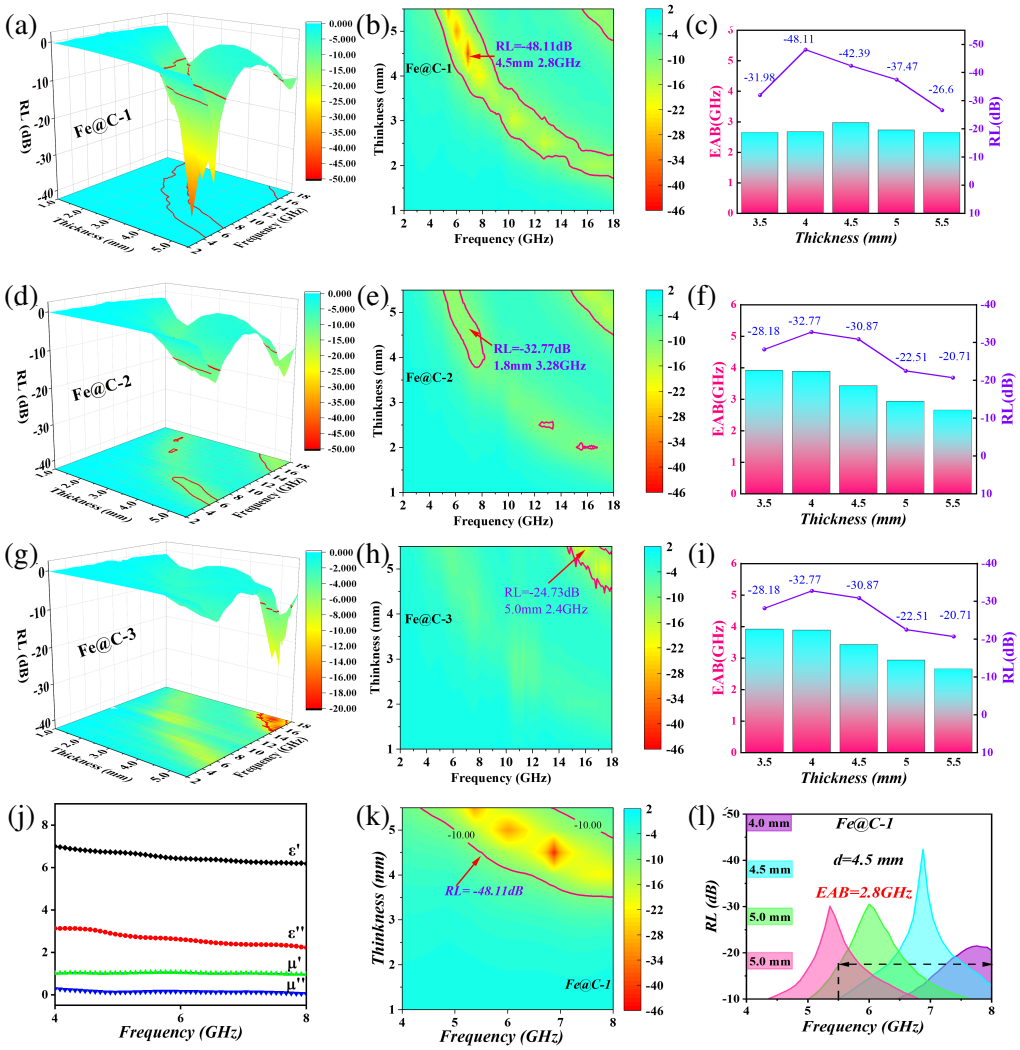


FIGURE 5. The Reflection loss (*RL*) performance of (a), (b), (c) Fe@C-1, (d), (e), (f) Fe@C-2, (h), (i), (j) Fe@C-3 composites. (k) Electromagnetic parameters, (l)2D *RL* mapping and (m) *RL* curves of Fe@C-1 in C-bands.

contribute to magnetic loss. The third involves the formation of numerous iron nanocrystals on the surface of carbon spheres. These nanocrystals create a multitude of magnetic flux lines and magnetic coupling, which further contribute to magnetic loss.

Being a crucial mechanism for microwave absorption, dielectric loss is mainly associated with conduction loss and polarization loss. These two components of dielectric loss are influenced by factors such as conductivity, interfaces, and dipoles [40]. Conductivity is mainly determined by the intrinsic conductivity of the composite material. As for Fe@C microspheres, both the carbon shell and Fe NPs exhibit considerable intrinsic conductive capabilities. Polarization loss typically includes three types: i. Intrinsic defects, caused by the absence or misplacement of crystal atoms. ii. Impurity defects produced by the introduction of impurity atoms. iii. Interfacial polarization [41].

Restricted magnetic diffusion results in a unique core-shell structure and provides an abundance of Fe-carbon heterogeneous interfaces, which can lead to enhanced interfacial polarization loss. High-density Fe nanocrystal alloy particles are encapsulated within a carbon matrix, resulting in carrier distribution areas surrounding the heterogeneous interfaces. These areas include both the carrier distribution area and the positive carrier distribution area, which contribute to the generation of interfacial polarization. The difference in Fermi level (EF) between body-centered cubic (bcc) Fe alloys (EF = 4.5 eV) [42] and carbon (EF = 5.00 eV) [43] at their interfaces leads to band bending and the formation of an internal electric field. This allows charges to migrate along the heterojunction interface from the Fe NPs to the carbon matrix.

Dipole polarization loss is another polarization mechanism where dipoles are formed due to asymmetric charge distribution in the material caused by defects. Under the action of an alternating magnetic field, these dipoles absorb energy and loosen, moving towards the direction of the electric field. However, the rotation of the dipoles cannot keep pace with the changing electric field, resulting in a phenomenon known as "polarization relaxation". Within the Fe@C microspheres, the Fe NPs experience compression from the surrounding carbon layer in the core-shell microstructure, resulting in the creation of numer-

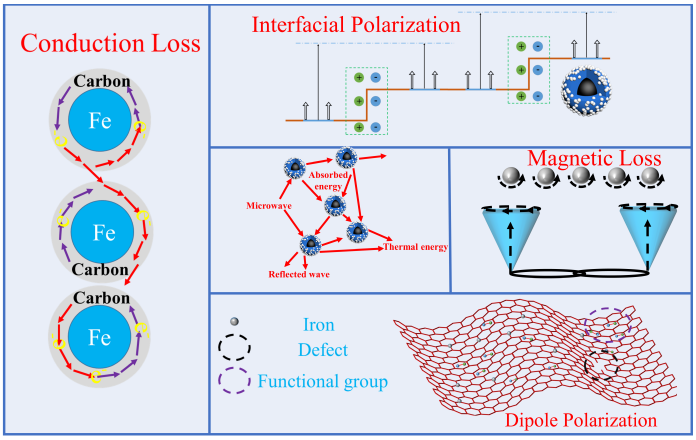


FIGURE 6. Schematic diagram of EM wave absorption mechanism in the Fe@C microspheres.

ous lattice defects. These defects are formed due to differential growth along the Fe (110) plane, resulting in significant grain boundaries. When interacting with incident alternating electromagnetic waves, the lattice distortion can effectively induce considerable amount of dipole polarization, thereby further dissipating microwave energy. This process enhances the interaction between the electric field and the molecules of the microspheres, thereby improving their ability to absorption electromagnetic waves

4. CONCLUSION

In summary, this study is dedicated to the development of magnetic-dielectric synergy Fe@C microspheres with the purpose of attaining exceptional electromagnetic wave absorption properties specifically in the C-band frequency range. The spray pyrolysis strategy was employed to effectively embed iron metal particles within the carbon shell. The utilization of melamine in varying concentrations had a notable impact on both the *RL* properties and the bandwidth of microwave absorption. The minimum *RL* value of Fe@C-1 microspheres can achieve -48.11 dB, covering approximately 70% of the C-band frequency range, with strong and wide bandwidth absorption capabilities. The Fe@C microspheres have enormous potential for large-scale production and are suitable for the application in electromagnetic wave absorption applications.

ACKNOWLEDGEMENT

This work was supported by the National Natural Science Foundation of China (52231007,12327804, T2321003,22088101), the Ministry of Science and Technology of China (973 Project No. 2021YFA1200600) and the Shanghai Sailing Program (22YF1447800)

REFERENCES

[1] Li, X., X. Qu, Z. Xu, W. Dong, F. Wang, W. Guo, H. Wang, and Y. Du, "Fabrication of three-dimensional flower-like heterogeneous Fe3O4/Fe particles with tunable chemical composition and microwave absorption performance," *ACS Applied Materials & Interfaces*, Vol. 11, No. 21, 19 267–19 276, 2019.

[2] Huang, M., L. Wang, K. Pei, B. Li, W. You, L. Yang, G. Zhou, J. Zhang, C. Liang, and R. Che, "Heterogeneous interface engineering of bi-metal MOFs-derived ZnFe2O4–ZnO-Fe@C microspheres via confined growth strategy toward superior electromagnetic wave absorption," *Advanced Functional Materials*, Vol. 34, No. 3, 2308898, 2024.

[3] Wang, L., M. Huang, K. Pei, W. You, B. Zhao, L. Wu, C. Liang, J. Zhang, and R. Che, "Confined magnetic vortex motion from metal-organic frameworks derived Ni@ C microspheres boosts electromagnetic wave energy dissipation," *Advanced Powder Materials*, Vol. 2, No. 3, 100111, 2023.

[4] Xing, C., S. Zhu, Z. Ullah, X. Pan, F. Wu, X. Zuo, J. Liu, M. Chen, W. Li, Q. Li, and L. Liu, "Ultralight and flexible graphene foam coated with Bacillus subtilis as a highly efficient electromagnetic interference shielding film," *Applied Surface Science*, Vol. 491, 616–623, 2019.

[5] Qiang, R., Y. Du, H. Zhao, Y. Wang, C. Tian, Z. Li, X. Han, and P. Xu, "Metal organic framework-derived Fe/C nanocubes toward efficient microwave absorption," *Journal of Materials Chemistry A*, Vol. 3, No. 25, 13 426–13 434, 2015.

[6] Qiu, Y., Y. Lin, H. Yang, L. Wang, M. Wang, and B. Wen, "Hollow Ni/C microspheres derived from Ni-metal organic framework for electromagnetic wave absorption," *Chemical Engineering Journal*, Vol. 383, 123207, 2020.

[7] Wang, T., H. Wang, X. Chi, R. Li, and J. Wang, "Synthesis and microwave absorption properties of Fe–C nanofibers by electrospinning with disperse Fe nanoparticles parceled by carbon," *Carbon*, Vol. 74, 312–318, 2014.

[8] Wang, F., Y. Sun, D. Li, B. Zhong, Z. Wu, S. Zuo, D. Yan, R. Zhuo, J. Feng, and P. Yan, "Microwave absorption properties of 3D cross-linked Fe/C porous nanofibers prepared by electrospinning," *Carbon*, Vol. 134, 264–273, 2018.

[9] Guo, Z., R. Zhan, Y. Shi, D. Zhu, J. Pan, C. Yang, Y. Wang, and J. Wang, "Innovative and green utilization of zinc-bearing dust by hydrogen reduction: Recovery of zinc and lead, and synergetic preparation of Fe/C micro-electrolysis materials," *Chemical Engineering Journal*, Vol. 456, 141157, 2023.

[10] Liu, Q., X. Liu, H. Feng, H. Shui, and R. Yu, "Metal organic framework-derived Fe/carbon porous composite with low Fe content for lightweight and highly efficient electromagnetic wave absorber," *Chemical Engineering Journal*, Vol. 314, 320–327, 2017.

[11] Fei, Y. and E. Brosh, "Experimental study and thermodynamic calculations of phase relations in the Fe–C system at high pressure," *Earth and Planetary Science Letters*, Vol. 408, 155–162, 2014.

[12] Park, J. B., S. H. Jeong, M. S. Jeong, J. Y. Kim, and B. K. Cho, "Synthesis of carbon-encapsulated magnetic nanoparticles by pulsed laser irradiation of solution," *Carbon*, Vol. 46, No. 11, 1369–1377, 2008.

[13] Borysiuk, J., A. Grabias, J. Szczytko, M. Bystrzejewski, A. Twardowski, and H. Lange, "Structure and magnetic properties of carbon encapsulated Fe nanoparticles obtained by arc plasma and combustion synthesis," *Carbon*, Vol. 46, No. 13, 1693–1701, 2008.

[14] Lou, Z., Y. Li, H. Han, H. Ma, L. Wang, J. Cai, L. Yang, C. Yuan, and J. Zou, "Synthesis of porous 3D Fe/C composites from waste wood with tunable and excellent electromagnetic wave absorption performance," *ACS Sustainable Chemistry & Engineering*, Vol. 6, No. 11, 15 598–15 607, 2018.

[15] Li, X.-P., Z. Deng, Y. Li, H.-B. Zhang, S. Zhao, Y. Zhang, X.-Y. Wu, and Z.-Z. Yu, "Controllable synthesis of hollow microspheres with Fe@ Carbon dual-shells for broad bandwidth microwave absorption," *Carbon*, Vol. 147, 172–181, 2019.

[16] Liu, Q., B. Cao, C. Feng, W. Zhang, S. Zhu, and D. Zhang, "High permittivity and microwave absorption of porous graphitic carbons encapsulating Fe nanoparticles," *Composites Science and Technology*, Vol. 72, No. 13, 1632–1636, 2012.

[17] Yang, F., G. Jiang, F. Yan, and Q. Chang, "Fe/C magnetic nanocubes with enhanced peroxidase mimetic activity for colorimetric determination of hydrogen peroxide and glucose," *Microchimica Acta*, Vol. 186, 1–8, 2019.

[18] Dong, S., J. Li, S. Zhang, N. Li, B. Li, Q. Zhang, and L. Ge, "Excellent microwave absorption performance of PAN-based Fe/C nanofibers with low loading fillers," *Colloids and Surfaces A: Physicochemical and Engineering Aspects*, Vol. 655, 130280, 2022.

[19] Zhang, J., Q. Kong, and D.-Y. Wang, "Simultaneously improving the fire safety and mechanical properties of epoxy resin with Fe-CNTs via large-scale preparation," *Journal of Materials Chemistry A*, Vol. 6, No. 15, 6376–6386, 2018.

[20] Abdullaeva, Z., E. Omurzak, C. Iwamoto, H. S. Ganapathy, S. Sulaimankulova, C. Liliang, and T. Mashimo, "Onion-like carbon-encapsulated Co, Ni, and Fe magnetic nanoparticles with low cytotoxicity synthesized by a pulsed plasma in a liquid," *Carbon*, Vol. 50, No. 5, 1776–1785, 2012.

[21] Bao, S., M. Zhang, X. Bu, W. Zhang, Z. Jiang, and Z. Xie, "Combinatorial structural engineering of multichannel hierarchical hollow microspheres assembled from centripetal Fe/C nanosheets to achieve effective integration of sound absorption and microwave absorption," *ACS Applied Materials & Interfaces*, Vol. 15, No. 10, 13 565–13 575, 2023.

[22] Mao, R., S. Bao, Q. Li, Y. Yuan, Z. Liang, M. Zhang, Z. Jiang, and Z. Xie, "Rational design of two-dimensional flaky Fe/void/C composites for enhanced microwave absorption properties," *Dalton Transactions*, Vol. 51, No. 22, 8705–8713, 2022.

[23] Lou, Z., Y. Li, H. Han, H. Ma, L. Wang, J. Cai, L. Yang, C. Yuan, and J. Zou, "Synthesis of porous 3D Fe/C composites from waste wood with tunable and excellent electromagnetic wave absorption performance," *ACS Sustainable Chemistry & Engineering*, Vol. 6, No. 11, 15 598–15 607, 2018.

[24] Gao, S., G. Zhang, Y. Wang, X. Han, Y. Huang, and P. Liu, "MOFs derived magnetic porous carbon microspheres constructed by core-shell Ni@ C with high-performance microwave absorption," *Journal of Materials Science & Technology*, Vol. 88, 56–65, 2021.

[25] Chai, L., Y. Wang, N. Zhou, Y. Du, X. Zeng, S. Zhou, Q. He, and G. Wu, "In-situ growth of core-shell ZnFe2O4@ porous hollow carbon microspheres as an efficient microwave absorber," *Journal of Colloid and Interface Science*, Vol. 581, 475–484, 2021.

[26] Wang, L., M. Huang, X. Qian, L. Liu, W. You, J. Zhang, M. Wang, and R. Che, "Confined magnetic-dielectric balance boosted electromagnetic wave absorption," *Small*, Vol. 17, No. 30, 2100970, 2021.

[27] Wang, Y.-L., S.-H. Yang, H.-Y. Wang, G.-S. Wang, X.-B. Sun, and P.-G. Yin, "Hollow porous CoNi/C composite nanomaterials derived from MOFs for efficient and lightweight electromagnetic wave absorber," *Carbon*, Vol. 167, 485–494, 2020.

[28] Zhang, X., M. Liu, J. Xu, Q. Ouyang, C. Zhu, X. Zhang, X. Zhang, and Y. Chen, "Flexible and waterproof nitrogen-doped carbon nanotube arrays on cotton-derived carbon fiber for electromagnetic wave absorption and electric-thermal conversion," *Chemical Engineering Journal*, Vol. 433, 133794, 2022.

[29] Huang, J., J. Qin, Q. Meng, L. Wang, Y. Du, and S. Z. Shen, "Flexible free-standing BixSey@ C/PEDOT: PSS thermoelectric composite film with high-performance electromagnetic interference shielding," *Applied Surface Science*, Vol. 639, 158162, 2023.

[30] Stephen, C., B. Shivamurthy, R. Selvam, S. R. Behara, A.-H. I. Mourad, and S. Kannan, "Design and finite element study of kevlar based combat helmet for protection against high-velocity impacts," *Materials Today: Proceedings*, Vol. 56, 3636–3641, 2022.

[31] Wang, P., L. Cheng, and L. Zhang, "One-dimensional carbon/SiC nanocomposites with tunable dielectric and broadband electromagnetic wave absorption properties," *Carbon*, Vol. 125, 207–220, 2017.

[32] Yang, L., H. Lv, M. Li, Y. zhang, J. Liu, and Z. Yang, "Multiple polarization effect of shell evolution on hierarchical hollow C@ MnO2 composites and their wideband electromagnetic wave absorption properties," *Chemical Engineering Journal*, Vol. 392, 123666, 2020.

[33] Garg, A., A. Goel, S. Prasher, R. Kumar, and R. Moulick, "Mxene nanocomposites for microwave absorption," in *Journal of Physics: Conference Series*, Vol. 2267, No. 1, 012084, 2022.

[34] Huo, J., L. Wang, and H. Yu, "Polymeric nanocomposites for electromagnetic wave absorption," *Journal of Materials Science*, Vol. 44, 3917–3927, 2009.

[35] Ren, F., H. Yu, L. Wang, M. Saleem, Z. Tian, and P. Ren, "Current progress on the modification of carbon nanotubes and their application in electromagnetic wave absorption," *RSC Advances*, Vol. 4, No. 28, 14 419–14 431, 2014.

[36] Wang, L., R. Mao, M. Huang, H. Jia, Y. Li, X. Li, Y. Cheng, J. Liu, J. Zhang, L. Wu, and R. Che, "Heterogeneous interface engineering of high-density MOFs-derived Co nanoparticles anchored on N-doped RGO toward wide-frequency electromagnetic wave absorption," *Materials Today Physics*, Vol. 35, 101128, 2023.

[37] Li, X., D. Du, C. Wang, H. Wang, and Z. Xu, "In situ synthesis of hierarchical rose-like porous Fe@ C with enhanced electromagnetic wave absorption," *Journal of Materials Chemistry C*, Vol. 6, No. 3, 558–567, 2018.

[38] Wang, X.-X., Q. Zheng, Y.-J. Zheng, and M.-S. Cao, "Green EMI shielding: Dielectric/magnetic "genes" and design philosophy," *Carbon*, Vol. 206, 124–141, 2023.

[39] Zheng, Q., J. Wang, M. Yu, W.-Q. Cao, H. Zhai, and M.-S. Cao, "Heterodimensional structure porous nanofibers embedded confining magnetic nanocrystals for electromagnetic functional ma-

terial and device," *Carbon*, Vol. 210, 118049, 2023.

[40] Chandrashekhar, V. G., T. Senthamarai, R. G. Kadam, O. Malina, J. Kašlík, R. Zbořil, M. B. Gawande, R. V. Jagadeesh, and M. Beller, "Silica-supported Fe/Fe–O nanoparticles for the catalytic hydrogenation of nitriles to amines in the presence of aluminium additives," *Nature Catalysis*, Vol. 5, No. 1, 20–29, 2022.

[41] Yan, J., Q. Zheng, S.-P. Wang, Y.-Z. Tian, W.-Q. Gong, F. Gao, J.-J. Qiu, L. Li, S.-H. Yang, and M.-S. Cao, "Multifunctional organic-inorganic hybrid perovskite microcrystalline engineering and electromagnetic response switching multi-band devices," *Advanced Materials*, Vol. 35, No. 25, 2300015, 2023.

[42] Cao, C., P. J. Hirschfeld, and H.-P. Cheng, "Proximity of antiferromagnetism and superconductivity in LaFeAsO1−xFx: Effective Hamiltonian from ab initio studies," *Physical Review B*, Vol. 77, No. 22, 220506, 2008.

[43] Chen, S., X. Zhou, J. Liao, S. Yang, X. Zhou, Q. Gao, S. Zhang, Y. Fang, X. Zhong, and S. Zhang, "FeNi intermetallic compound nanoparticles wrapped with N-doped graphitized carbon: A novel cocatalyst for boosting photocatalytic hydrogen evolution," *Journal of Materials Chemistry A*, Vol. 8, No. 6, 3481–3490, 2020.